

Exceptional flat bands in bipartite non-Hermitian quantum crystals

Juan Pablo Esparza^{1,2} and Vladimir Jurić^{1,*}

¹*Departamento de Física, Universidad Técnica Federico Santa María, Casilla 110, Valparaíso, Chile*

²*Instituto de Física, Pontificia Universidad Católica de Valparaíso, Avenida Universidad 331, Curauma, Valparaíso, Chile*

Flat bands, in which kinetic energy is quenched and quantum states become macroscopically degenerate, host a rich variety of correlated and topological phases, from unconventional superconductors to fractional Chern insulators. In Hermitian lattices, their formation mechanisms are now well understood, but whether such states persist, and acquire new features in non-Hermitian (NH) quantum crystals, relevant to open and driven systems, has remained an open question. Here we show that the Hermitian principle for flat-band formation in bipartite lattices, based on a sublattice degeneracy mismatch, extends directly to the NH regime: whenever one sublattice hosts a momentum-independent eigenvalue with degeneracy exceeding that of its partner on the other sublattice, flat bands arise regardless of gain, loss, or complex couplings. Strikingly, at exceptional points, dispersive bands coalesce to form *exceptional flat bands* that persist beyond these singularities, exhibiting biorthogonal eigenmodes spanning both sublattices, with energies and lifetimes tunable via sublattice asymmetry and non-reciprocal couplings. This general framework unifies Hermitian and NH flat-band constructions, and reveals dispersionless states with no closed-system analogue. The proposed construction is applicable to synthetic platforms, from classical metamaterials, where flat bands can be directly emulated, to quantum-engineered systems such as photonic crystals and ultracold atom arrays, which should host correlated and topological phases emerging from such exceptional flat bands.

Flat electronic bands, where kinetic energy is completely quenched and quantum states exhibit a macroscopic degeneracy, are fertile ground for unconventional superconductivity, fractional Chern insulators, and other exotic many-body phases [1–13]. The theoretical proposals [14–16] and experimental discovery [6, 7] of nearly dispersionless bands in twisted bilayer graphene (TBG) revealed the powerful role of symmetry and topology in stabilizing such states [17, 18], sparking intense efforts to design flat-band systems across condensed matter [19–24], metamaterials [25–27], photonics [28–31], and ultracold atomic platforms [32–35]. While the symmetry-based mechanisms behind flat bands in Hermitian crystals are now well understood [36–39], their fate in the fundamentally different setting of non-Hermitian (NH) quantum matter, relevant to open and out-of-equilibrium systems, remains largely unexplored [40–51].

NH physics, characterized by complex spectra, asymmetric couplings and engineered gain–loss, has become a central theme in synthetic and open quantum matter [52–54]. It departs from Hermitian band theory through two hallmark phenomena: (i) exceptional points, where eigenvalues and eigenvectors coalesce, enabling anomalous transport and topological spectral flows [55–59]; and (ii) the NH skin effect, in which a macroscopic number of modes pile up at the boundary due to non-reciprocity and spectral winding [52, 54]. This endeavor has recently pushed to the interacting Dirac materials [60–64], opening a new frontier where NH effects intertwine with strong correlations. Yet, despite reshaping our understanding of band topology, these advances have left open a central question: can flat bands, long celebrated in Hermitian systems for hosting correlated and topological

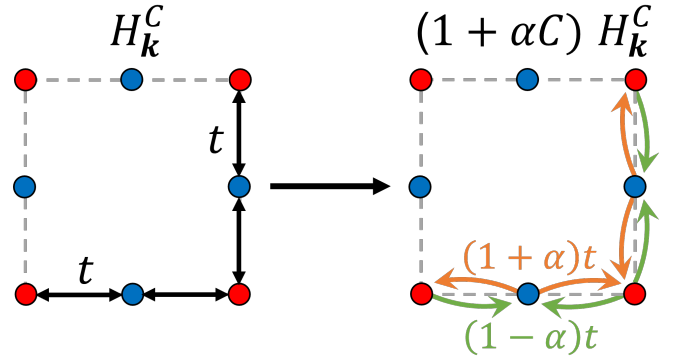


FIG. 1. Left: the square Lieb lattice with three inequivalent sites in the unit cell, forming two sublattices, L_A (blue dots) and L_B (red dots), with the flat band arising due to the imbalance in the number of sites belonging to each sublattice, with $N_A = 2$ and $N_B = 1$. Right: the non-Hermitian crystal obtained by exploiting the inherent particle-hole symmetry of the original lattice (C), where the new contribution acquires the form of a non-reciprocal hopping between nearest neighbors.

phases, persist and acquire distinctive signatures in this NH landscape?

Initial insight came from NH generalizations of twisted bilayer graphene (TBG), where it was shown that flat bands can emerge at *exceptional magic angles* due to spectral collapse at NH degeneracies [65]. These findings suggested that non-Hermiticity could stabilize flat bands in crystalline systems under specific conditions, a possibility further supported by model-based studies across photonic and electronic platforms [40, 41, 44, 45, 50, 51,

[66]. However, a general and symmetry-based framework capable of predicting and engineering such flat bands has so far been lacking.

Here we show that the Hermitian principle for flat-band formation in bipartite lattices [37], based on a sublattice degeneracy mismatch, extends directly to the NH regime: whenever one sublattice hosts a momentum-independent eigenvalue with degeneracy exceeding that of its counterpart at other sublattice, flat bands arise irrespective of the specific NH effects, including gain, loss, or complex-valued couplings. Strikingly, dispersive bands coalesce at exceptional points and moreover persist as flat modes beyond these spectral singularities, yielding *exceptional flat bands* with biorthogonal eigenmodes spanning both sublattices. Their energy and lifetime can be continuously tuned via sublattice asymmetries, and intra-sublattice hoppings. We showcase its versatility through examples from NH Lieb lattices, showing a geometric imprint of the exceptional flat bands on the quantum metric (Fig. 2), to realistic multi-band models (Figs. 3-5), highlighting its applicability across diverse synthetic platforms. Because it depends only on sublattice structure, the principle is directly relevant to photonic crystals with engineered gain-loss profiles [52, 67–71], ultracold atomic arrays with tailored dissipation [72–76], and metamaterials [77–83]. By providing a general prescription for flat-band engineering in open quantum matter, our results pave the systematic way for realizing interaction-driven and topological phases far from equilibrium. [60–64, 84–96].

General construction principle. Flat bands naturally arise in Hermitian bipartite crystalline lattices (BCLs), where two interpenetrating sublattices, L_A and L_B , host different numbers of degrees of freedom per unit cell, N_A and N_B , respectively [37]. In momentum space, the Bloch Hamiltonian assumes a block form

$$H_{\mathbf{k}} = \begin{pmatrix} A_{\mathbf{k}} & S_{\mathbf{k}} \\ S_{\mathbf{k}}^\dagger & B_{\mathbf{k}} \end{pmatrix}, \quad (1)$$

with $A_{\mathbf{k}}$ and $B_{\mathbf{k}}$ describing intra-sublattice hoppings and $S_{\mathbf{k}}$ the inter-sublattice hybridization. If $A_{\mathbf{k}}$ hosts a momentum-independent eigenvalue ϵ_a with degeneracy $n_a > N_B$, the coupling $S_{\mathbf{k}}$ cannot fully hybridize these modes with L_B , leaving a kernel of dimension $(n_a - N_B)$ that manifests as dispersionless bands at energy ϵ_a , independent of $B_{\mathbf{k}}$.

The main wisdom regarding the generalization of this principle to the NH realm is provided by the chiral BCL

$$H_{\mathbf{k}}^{\mathcal{C}} = \begin{pmatrix} 0 & S_{\mathbf{k}} \\ S_{\mathbf{k}}^\dagger & 0 \end{pmatrix}, \quad (2)$$

with at least $(N_A - N_B)$ flat bands [97], possessing the chiral (sublattice or unitary particle-hole) symmetry, $\{\mathcal{C}, H_{\mathbf{k}}^{\mathcal{C}}\} = 0$, with the chiral operator

$$\mathcal{C} = \begin{pmatrix} \mathbf{1}_{N_A} & 0 \\ 0 & -\mathbf{1}_{N_B} \end{pmatrix}, \quad (3)$$

where $\mathbf{1}_n$ is the unitary $n \times n$ matrix. Therefore, $(\mathcal{C}H_{\mathbf{k}}^{\mathcal{C}})^\dagger = -\mathcal{C}H_{\mathbf{k}}^{\mathcal{C}}$, implying that the operator $\mathcal{C}H_{\mathbf{k}}^{\mathcal{C}}$ is anti-Hermitian. Consequently, we use this operator to construct the NH deformation of the chiral-symmetric Hermitian Hamiltonian $H_{\mathbf{k}}^{\mathcal{C}}$,

$$H_{\mathbf{k}} = (1 + \alpha\mathcal{C})H_{\mathbf{k}}^{\mathcal{C}} = \begin{pmatrix} 0 & (1 + \alpha)S_{\mathbf{k}} \\ (1 - \alpha)S_{\mathbf{k}}^\dagger & 0 \end{pmatrix}, \quad (4)$$

where $\alpha \in \mathbb{R}$ quantifies the non-Hermiticity. Notice that the chiral operator \mathcal{C} plays the role analogous to the mass term in the case of NH Dirac Hamiltonian [60] since it anticommutes with the parent Hermitian Hamiltonian, $H_{\mathbf{k}}^{\mathcal{C}}$. Such deformation leaves the original flat bands intact while introducing NH spectral features, as we show in the following.

To this end, we can express the eigenvalues and eigenstates of such Hamiltonian in terms of the singular eigenstates of $S_{\mathbf{k}}$ and $S_{\mathbf{k}}^\dagger$, denoted by $\psi_{n,\mathbf{k}}$ and $\phi_{n,\mathbf{k}}$, respectively, for $1 \leq n \leq r_{\mathbf{k}}$, with $r_{\mathbf{k}} \leq N_B$ as the rank of $S_{\mathbf{k}}$, both with corresponding eigenvalue $\epsilon_{n,\mathbf{k}} \in \mathbb{R}$, and related as $S_{\mathbf{k}}^\dagger \phi_{n,\mathbf{k}} = \epsilon_{n,\mathbf{k}} \psi_{n,\mathbf{k}}$ and $S_{\mathbf{k}} \psi_{n,\mathbf{k}} = \epsilon_{n,\mathbf{k}} \phi_{n,\mathbf{k}}$. Then, the system have $2r_{\mathbf{k}}$ dispersive right-eigenstates of $H_{\mathbf{k}}$, given by

$$\Psi_{n,\mathbf{k},R}^\pm = \frac{1}{\sqrt{2\sqrt{1-\alpha^2}}} \begin{pmatrix} \pm\sqrt{1+\alpha}\phi_{n,\mathbf{k}} \\ \sqrt{1-\alpha}\psi_{n,\mathbf{k}} \end{pmatrix}, \quad (5)$$

with the dispersion

$$E_{n,\mathbf{k}}^\pm = \pm\sqrt{1-\alpha^2}\epsilon_{n,\mathbf{k}}, \quad (6)$$

for $1 \leq n \leq r_{\mathbf{k}}$. The corresponding left-eigenstates can be obtained immediately by the substitution $\alpha \rightarrow -\alpha$, and the normalization factor is chosen to satisfy the biorthogonal condition $\Psi_{\mathbf{k},L}^\dagger \Psi_{\mathbf{k},R} = 1$, see also Sec. S1 of the Supplementary Materials (SM) [98]. At the exceptional points ($|\alpha| = 1$), the dispersive branches therefore coalesce producing *exceptional flat bands* with biorthogonal states. Furthermore, beyond these spectral singularities, for $|\alpha| > 1$, these modes persist, remaining dispersionless while acquiring finite lifetimes as their energies turn purely imaginary.

To extend this construction, we break the chiral symmetry via asymmetric chemical potentials $\mu_{A,B} = \bar{\mu} \pm \delta\mu$ modifying the Hamiltonian to

$$H_{\mathbf{k}} = \begin{pmatrix} \mu_A \mathbf{1}_{N_A} & (1 + \alpha)S_{\mathbf{k}} \\ (1 - \alpha)S_{\mathbf{k}}^\dagger & \mu_B \mathbf{1}_{N_B} \end{pmatrix}, \quad (7)$$

with the spectrum $E_{n,\mathbf{k}}^\pm = \bar{\mu} \pm \Delta_{\mathbf{k}}$, where $\Delta_{\mathbf{k}} = \sqrt{\delta\mu^2 + (1 - \alpha^2)\epsilon_{n,\mathbf{k}}^2}$. The flat bands are therefore shifted to μ_A or μ_B while preserving their degeneracy. At the exceptional points, dispersive states again collapse, populating an additional flat band pinned at the average chemical potential $\bar{\mu}$. This collapse occurs even when $S_{\mathbf{k}}$ is full rank, producing flat states supported on

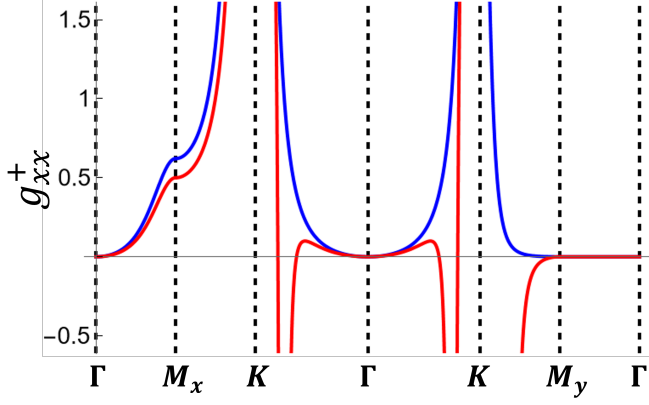


FIG. 2. The diagonal element of the quantum metric in the Lieb lattice model with unbalanced chemical potential for $\alpha = 0$ (blue) and $\alpha = 1.1$ (red). See Eq. (9). In both cases, there is a divergence at the K -point due to the standard band-touching, but the NH model exhibits an additional purely NH induced divergence to *negative* infinity, where $g_{xx}^+ \rightarrow -\infty$, due to the spectral collapse onto the exceptional flat band pinned at $\delta\mu = 0.5$. See Sec. S3 of the SM for the details of the model. We here set $t = 1$.

both sublattices, representing a hallmark of NH physics. See also Sec. S1. For $|\alpha| > 1$, these states become long-lived, nearly dispersionless modes. Thus, the construction principle remains operative: whenever one sublattice hosts a momentum-independent eigenvalue whose degeneracy exceeds the dimensionality of its complement, flat bands necessarily emerge. In the NH regime, exceptional points induce spectral collapse, generating additional flat modes with no Hermitian counterpart, as can be seen in Fig. 4.

Generalized NH BCL. We next explore the flat-band principle in its most general bipartite form, where a single sublattice hosts a momentum-independent eigenvalue while its counterpart carries arbitrary form. The Hamiltonian can be written as

$$H_{\mathbf{k}} = \begin{pmatrix} \epsilon_a \mathbf{1}_{N_A} & (1 + \alpha)S_{\mathbf{k}} \\ (1 - \alpha)S_{\mathbf{k}}^\dagger & B_{\mathbf{k}} \end{pmatrix}, \quad (8)$$

where $B_{\mathbf{k}}$ represents an arbitrary, momentum-dependent intra-sublattice operator. In this case, the flat bands associated with the kernel of $S_{\mathbf{k}}^\dagger$ remain pinned at $E_{n,\mathbf{k}} = \epsilon_a$, since their existence relies only on the degeneracy mismatch and the singular structure of $S_{\mathbf{k}}$, which are unaffected by the NH deformation. However, unlike in the chiral or symmetric cases, the presence of $B_{\mathbf{k}}$ introduces nontrivial momentum dependence into the dispersive sector. As a result, even at the exceptional points $\alpha = \pm 1$, the dispersive bands do not necessarily collapse onto the flat bands. The spectral flattening observed in simpler models is thus no longer guaranteed, as it depends on the detailed structure of $B_{\mathbf{k}}$.

Topological aspects. To probe the geometric properties of the exceptional flat bands, we evaluate the NH

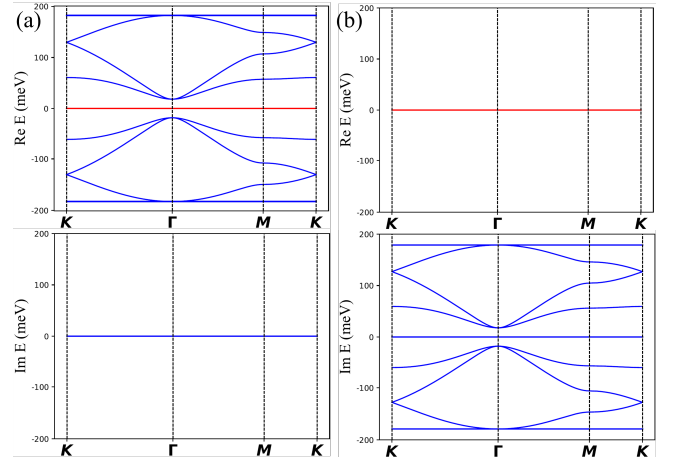


FIG. 3. Real (top) and imaginary (bottom) part of the energy bands for the chiral ($\mu_A = \mu_B = 0$) model for $\alpha = 0$ (a) and $\alpha = 1.4$ (b), with the same parameters employed in Ref. [18]. In red, the degenerate flat band pinned at zero energy due to the difference between sublattices' sites, $N_A - N_B = 2$. As elaborated in the main text, for this case the spectrum becomes purely imaginary beyond the exceptional point $\alpha > 1$, and thus all the states collapse onto the zero-energy level.

quantum geometric tensor (QGT) [99–101],

$$Q_{\mu\nu}^n = \langle \partial_\mu \psi_n^L | \partial_\nu \psi_n^R \rangle - \langle \partial_\mu \psi_n^L | \psi_n^R \rangle \langle \psi_n^L | \partial_\nu \psi_n^R \rangle, \quad (9)$$

whose real and imaginary parts define the quantum metric, $g_{\mu\nu}^n = \text{Re } Q_{\mu\nu}^n$, and the Berry curvature, $F_{\mu\nu}^n = -2 \text{Im } Q_{\mu\nu}^n$, respectively.

In chiral NH BCLs, the deformation acts as a global prefactor without altering the momentum dependence of the eigenstates. Consequently, the Berry curvature vanishes, and the flat bands inherit the trivial topological character of their Hermitian counterparts [37, 102]. This behavior persists even in the presence of sublattice-asymmetric chemical potentials and at exceptional points: the left- and right-eigenstates remain identical to those of the Hermitian model, preventing the generation of new topological invariants.

Nevertheless, the quantum metric exhibits a distinct and experimentally relevant sensitivity to NH effects. In particular, dispersive states in systems with finite chemical potential acquire a non-trivial α -dependence in $g_{\mu\nu}^n$ (see Sec. S2 of SM [98]). Since the quantum metric governs measurable responses such as optical absorption, this dependence provides a concrete route to detecting NH signatures in flat-band systems. Thus, while the addition of NH terms does not alter the conventional topological classification, it leaves a geometric imprint encoded in the quantum metric, such as an additional divergence close to high-symmetry points in the Brillouin zone, as shown in the case of a Lieb lattice model (see Sec. S3 of the SM [98]) in Fig. 2. Exploring such geometric responses opens a promising direction for uncovering

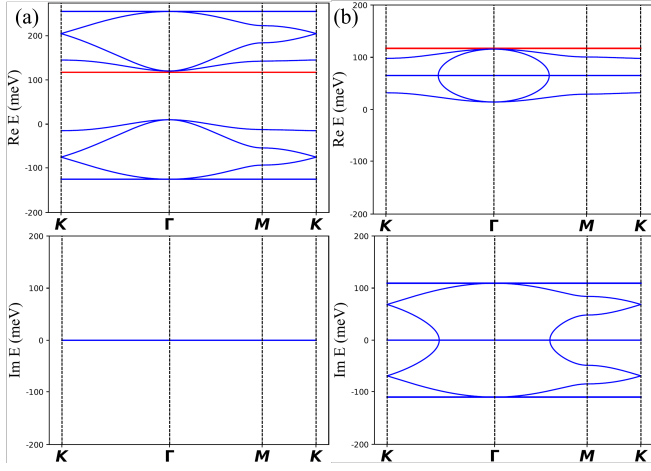


FIG. 4. Real (top) and imaginary (bottom) parts of the energy bands for the non-chiral model for $\mu_A = 117 \text{ meV}$ and $\mu_B = 13 \text{ meV}$ with $\alpha = 0$ (a) and $\alpha = 1.2$ (b). Notice that the full energy spectrum is shifted, and in particular the flat band (in red) is pinned at μ_A . Then, for $\alpha > 1$, the dispersive states begin to collapse on to the value $\bar{\mu} = 65 \text{ meV} < \mu_A$ for an extended region of the BZ.

experimentally accessible manifestations of NH flat-band physics.

Examples. To illustrate how our construction operates in realistic settings, we apply it to two representative models.

We first consider the ten-band model of TBG [18], by introducing nonreciprocal hopping between sublattices to realize a NH chiral BCL. As shown in Fig. 3, the spectrum evolves from being purely real to purely imaginary upon crossing the exceptional point at $\alpha = 1$. For $\alpha < 1$, the flat bands persist with reduced dispersion, shrinking by a factor $\sqrt{1 - \alpha^2} < 1$. When finite and unequal chemical potentials are applied to the sublattices, the flat bands shift in energy (Fig. 4). In this non-chiral configuration, the original flat band is pinned at μ_A for $\alpha < 1$, while tuning beyond the exceptional point populates an additional flat band centered at $\bar{\mu}$. This emergent band is energetically favorable when $\bar{\mu} < \mu_A$, and although its states acquire a finite lifetime, $\tau \sim 1/\text{Im } E$, (see Fig. 4), they get stabilized by becoming long-lived at momentum-dependent exceptional points $|\epsilon_{n,\mathbf{k}}| = |\delta\mu/\sqrt{1 - \alpha^2}|$.

As a second example, we consider the NH extension of the tight-binding model for $\text{Ca}_2\text{Ta}_2\text{O}_7$ in Ref. [37], with its dispersion shown in Fig. 5. Here, a large on-site energy imbalance ($\delta\mu \sim 5 \text{ eV}$) ensures that the standard Hermitian flat band, pinned at $\mu_A < \bar{\mu}$, remains energetically dominant. Importantly, due to the substantial chemical potential offset, the spectrum remains real over a broad range of $\alpha > 1$, indicating that the system undergoes unitary evolution despite NH deformation. Consequently, the flat-band physics is only weakly modified, demonstrating robustness against strong on-site asym-

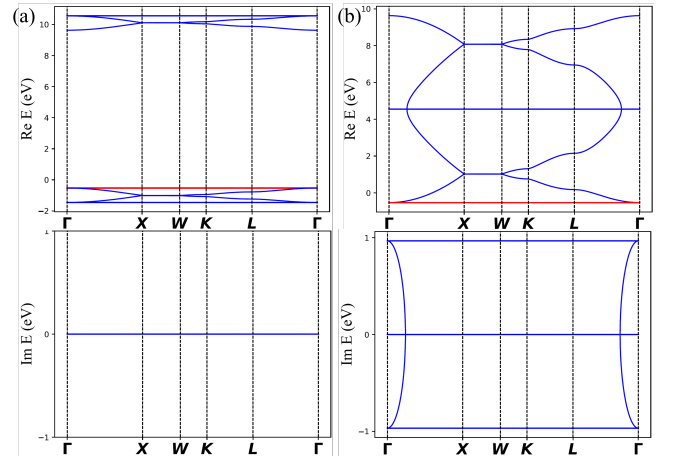


FIG. 5. Energy spectrum of the tight-binding model for the $\text{Ca}_2\text{Ta}_2\text{O}_7$ compound, with the hopping parameters in Ref. [37], for $\alpha = 0$ (a) and $\alpha = 1.9$ (b). For smaller values of α , the spectrum is still real-valued, due to the large gap between on-site energies, $\delta\mu \approx 5 \text{ eV}$. Here again the Hermitian flat band pinned at $\mu_A \approx -0.5 \text{ eV}$ is highlighted in red.

metry.

These examples highlight the versatility of our framework: it captures NH spectral collapse and the emergence of exceptional flat bands in systems with tunable asymmetry, while also describing regimes where conventional flat bands remain largely unaffected by the NH effects.

Discussion and outlook. We have shown that the flat-band mechanism, where a sublattice imbalance enforces dispersionless modes, carries over unchanged from the realm of Hermitian to NH quantum crystals. In this broader setting, the mechanism not only reproduces the Hermitian flat bands but also generates a distinct class of exceptional flat bands via spectral collapse at exceptional points, where dispersive modes collapse to form the exceptional flat bands. Their energies and lifetimes are tunable, with their biorthogonal eigenstates spanning both sublattices, features absent in closed systems

Photonic crystals with engineered gain-loss, ultracold-atom arrays with controlled dissipation, and non-reciprocal electronic metamaterials provide natural platforms for the NH BCLs considered here. In these settings, exceptional flat bands are expected to manifest via enhanced density of states, characteristic transport anomalies, and interaction-driven responses, thereby opening routes to correlated phases without Hermitian analogues. More broadly, the interplay of interactions, topology, and exceptional flat bands promises distinctive many-body phenomena in open quantum matter. Our symmetry-based construction offers a practical framework for flat-band engineering in NH materials and enables systematic exploration of strongly correlated and topological phases far from equilibrium.

Acknowledgment. We are grateful to Bitan Roy for

the critical reading of the manuscript. This work is supported by Fondecyt (Chile) Grant No. 1230933 (V.J.) and the Swedish Research Council Grant No. VR 2019-04735 (V.J.). J.P.E. acknowledges support from Agencia Nacional de Investigación y Desarrollo (ANID) – Scholarship Program through the Doctorado Nacional Grant No. 2024-21240412, and Dirección de Postgrado UTFSM through the PIIC Grant No. 28/2025.

Supplementary Material:

Exceptional flat bands in bipartite non-Hermitian quantum crystals

In this Supplementary Material we include: (S1) The explicit form of the eigenstates for the NH bipartite lattice both in the chiral case and with chemical potential offset at each sublattice; (S2) Details on the topological aspects displayed in terms of the quantum geometric tensor; (S3) A concrete example of our method applied to the Lieb lattice.

S1. Eigenproblem for the non-Hermitian Bipartite Lattices

To fully describe the quantum dynamics of the non-Hermitian (NH) bipartite crystalline lattice (BCL), we now solve the eigenvalue problem for the corresponding Bloch Hamiltonian obtained by the construction method illustrated in the main text. To do so, it becomes necessary to consider the right- and left-eigenproblem in order to construct the full biorthogonal basis for the Hilbert space, as

$$H_{\mathbf{k}}\Psi_{n,\mathbf{k},R} = E_{n,\mathbf{k}}\Psi_{n,\mathbf{k},R}, \quad \Psi_{n,\mathbf{k},L}^\dagger H_{\mathbf{k}} = E_{n,\mathbf{k}}\Psi_{n,\mathbf{k},L}^\dagger. \quad (10)$$

In this case, we can exploit the fact that $H_{\mathbf{k}}^\dagger(\alpha) = H_{\mathbf{k}}(-\alpha)$, thus is enough to just solve for the right-eigenvalue problem and then identify $\Psi_{n,\mathbf{k},L}(\alpha) \equiv \Psi_{n,\mathbf{k},R}(-\alpha)$ to obtain the complete set of eigenstates. It is also convenient for computational purposes to separate each eigenstate in two components, either with support on each of the sublattices as $\Psi_{n,\mathbf{k},R} = (\psi_A, \psi_B)^\top$, where ψ_α ($\alpha = A, B$) is a N_α -dimensional vector supported on the sublattice L_α . Therefore, the eigenvalue problem for the chiral case can be explicitly written as a system of equations in terms of the two components corresponding to two sublattices as

$$\begin{aligned} (1 + \alpha)S_{\mathbf{k}}\psi_B &= E_{n,\mathbf{k}}\psi_A, \\ (1 - \alpha)S_{\mathbf{k}}^\dagger\psi_A &= E_{n,\mathbf{k}}\psi_B. \end{aligned} \quad (11)$$

In this form is now useful to consider the singular value decomposition of the inter-sublattice operator $S_{\mathbf{k}} = \sum_n^{\gamma_{\mathbf{k}}} \epsilon_{n,\mathbf{k}} \phi_{n,\mathbf{k}} \psi_{n,\mathbf{k}}^\dagger$, where $\phi_{n,\mathbf{k}}$ ($\psi_{n,\mathbf{k}}$) is the left (right) singular eigenvector of $S_{\mathbf{k}}$ with eigenvalue $\epsilon_{n,\mathbf{k}}$, and they are related by the transformation

$$\begin{aligned} S_{\mathbf{k}}\psi_{n,\mathbf{k}} &= \epsilon_{n,\mathbf{k}}\phi_{n,\mathbf{k}}, \\ S_{\mathbf{k}}^\dagger\phi_{n,\mathbf{k}} &= \epsilon_{n,\mathbf{k}}\psi_{n,\mathbf{k}}. \end{aligned} \quad (12)$$

Away from the exceptional points, a direct comparison between Eqs. (11) and (12) leads to three different kinds of solutions, each one of them normalized in order to satisfy the biorthogonal condition $\Psi_L^\dagger \Psi_R = 1$:

1. $2r_{\mathbf{k}}$ dispersive states given by

$$\Psi_{n,\mathbf{k},R}^\pm = \frac{1}{\sqrt{2\sqrt{1-\alpha^2}}} \begin{pmatrix} \pm\sqrt{1+\alpha}\phi_{n,\mathbf{k}} \\ \sqrt{1-\alpha}\psi_{n,\mathbf{k}} \end{pmatrix},$$

with $E_{n,\mathbf{k}}^\pm = \pm\sqrt{1-\alpha^2}\epsilon_{n,\mathbf{k}}$.

2. $N_A - r_{\mathbf{k}}$ zero-modes given by the non-null kernel of $S_{\mathbf{k}}^\dagger$, as

$$\Psi_{n,\mathbf{k},R} = \begin{pmatrix} \phi_{n,\mathbf{k}} \\ 0 \end{pmatrix},$$

with $E_{n,\mathbf{k}} = 0$.

3. $N_B - r_{\mathbf{k}}$ zero-modes that arise when $S_{\mathbf{k}}$ is not full-rank, i.e. $r_{\mathbf{k}} < N_B$, given by

$$\Psi_{n,\mathbf{k},R} = \begin{pmatrix} 0 \\ \psi_{n,\mathbf{k}} \end{pmatrix},$$

with $E_{n,\mathbf{k}} = 0$.

Here, we assume normalization of the singular eigenstates $\psi_{n,\mathbf{k}}^\dagger \psi_{n,\mathbf{k}} = \phi_{n,\mathbf{k}}^\dagger \phi_{n,\mathbf{k}} = 1$. This is shown in Eqs. (5) and (6) in the main text.

Remarkably, the flat-band states retain the same form as in the Hermitian case [37], and the NH contribution only affects the dispersive states, that acquire an explicit dependence on α , becoming also ill-defined at the EPs $|\alpha| = 1$ due to normalization. At such points, the Hamiltonian becomes explicitly defective, acquiring a Jordan-block form, and therefore all eigenstates coalesce onto the flat-band eigenvalue. Beyond them, the dispersive bands become purely imaginary, so eventually all the dispersive states collapse to the zero-energy band, albeit with a finite lifetime.

We now break the chiral symmetry by adding chemical potential μ_α at each sublattice, $\alpha = A, B$. Eq. (10) is then modified as

$$\begin{aligned} (1 + \alpha)S_{\mathbf{k}}\psi_B &= (E_{n,\mathbf{k}} - \mu_A)\psi_A, \\ (1 - \alpha)S_{\mathbf{k}}^\dagger\psi_A &= (E_{n,\mathbf{k}} - \mu_B)\psi_B. \end{aligned} \quad (13)$$

Repeating the same strategy as in the previous case, we can compare Eqs. (13) and (12) to write the solution of the eigenproblem for the Hamiltonian in terms of the singular eigenstates and eigenvalues of $S_{\mathbf{k}}$, taking $|\alpha| \neq 1$. Such procedure yields again three kinds of solutions, that can be explicitly written in terms of the average chemical potential $\bar{\mu} = (\mu_A + \mu_B)/2$, the offset $\delta\mu = (\mu_A - \mu_B)/2$ and $\Delta_{\mathbf{k}} = \sqrt{\delta\mu^2 + (1 - \alpha^2)\epsilon_{n,\mathbf{k}}^2}$ as:

1. $2r_{\mathbf{k}}$ dispersive states given by

$$\Psi_{n,\mathbf{k},R}^\pm = \frac{1}{\sqrt{(\delta\mu \pm \Delta_{\mathbf{k}})^2 + (1 - \alpha^2)\epsilon_{n,\mathbf{k}}^2}} \begin{pmatrix} (\delta\mu \pm \Delta_{\mathbf{k}})\phi_{n,\mathbf{k}} \\ (1 - \alpha)\epsilon_{n,\mathbf{k}}\psi_{n,\mathbf{k}} \end{pmatrix},$$

with $E_{n,\mathbf{k}}^\pm = \bar{\mu} \pm \Delta_{\mathbf{k}}$.

2. $N_A - r_{\mathbf{k}}$ flat-band states given by

$$\Psi_{n,\mathbf{k},R} = \begin{pmatrix} \phi_{n,\mathbf{k}} \\ 0 \end{pmatrix},$$

with $E_{n,\mathbf{k}} = \mu_A$.

3. $N_B - r_{\mathbf{k}}$ flat-band states when $S_{\mathbf{k}}$ is not full-rank given by

$$\Psi_{n,\mathbf{k},R} = \begin{pmatrix} 0 \\ \psi_{n,\mathbf{k}} \end{pmatrix},$$

with $E_{n,\mathbf{k}} = \mu_B$.

Here the standard flat-band states that depend only on the sublattice imbalance $N_A - N_B \neq 0$ retain exactly their Hermitian form. By contrast, the dispersive sector acquires a non-trivial α -dependence which, together with its momentum dependence, yields a richer pattern of band flattening as the bands become complex. Specifically, two types of collapse occur: (i) at the exceptional points $\alpha = \pm 1$, the dispersive branches collapse onto the flat band $E_{n,\mathbf{k}} = \mu_{\alpha}$; and (ii) when $|\alpha| > |\delta\mu/\epsilon_{n,\mathbf{k}}|$, or equivalently when $\Delta_{\mathbf{k}} \in \mathbb{C}$, an NH spectral collapse produces complex-valued flat bands pinned at $\bar{\mu}$, which we term *exceptional flat bands*. Notably, at each exceptional point the resulting flat-band states have support on both sublattices, as seen from the explicit form of the dispersive eigenstates at $\alpha = \pm 1$.

S2. Quantum Geometric Tensor

To analyze the topological nature of the NH models constructed using our general principle, we employ the standard NH generalization of the Quantum Geometric Tensor (QGT), constructed in terms of the biorthogonal eigenstates of the Bloch Hamiltonian as

$$Q_{\mu\nu}^n = \langle \partial_{\mu} \psi_n^L | \partial_{\nu} \psi_n^R \rangle - \langle \partial_{\mu} \psi_n^L | \psi_n^R \rangle \langle \psi_n^L | \partial_{\nu} \psi_n^R \rangle, \quad (14)$$

where $|\psi_n^{\alpha}\rangle$ with $\alpha = R$ ($\alpha = L$) refers to the n -th right-(left)-eigenstate of $H_{\mathbf{k}}$ and $\partial_{\mu} \equiv \partial/\partial k_{\mu}$. The QGT encodes both the geometrical and topological properties of a given system in terms of the quantum metric $g_{\mu\nu}^n = \text{Re } Q_{\mu\nu}^n$ and the Berry curvature $F_{\mu\nu}^n = -2 \text{Im } Q_{\mu\nu}^n$, respectively.

First, for the chiral NH BCL, the dispersive eigenstates factorize: their momentum dependence separates from the NH parameter α . Consequently, when the QGT is evaluated via Eq. (14), the α -dependent factors cancel in the inner products and the NH contribution vanishes

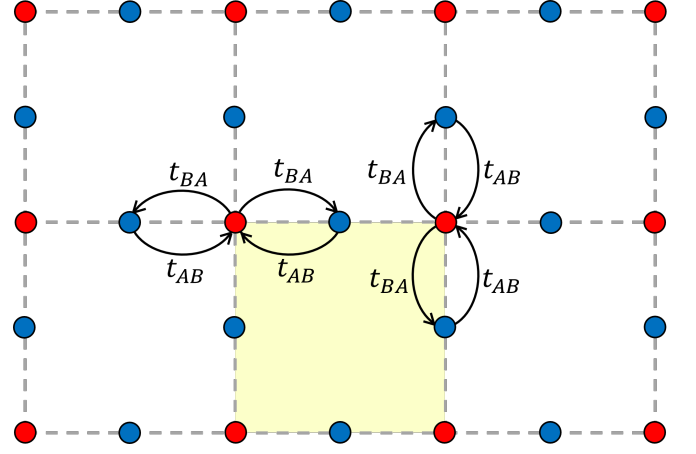


FIG. 6. Two-dimensional non-Hermitian Lieb lattice. The unit cell is highlighted in yellow. Blue dots form sublattice L_A with $N_A = 2$ sites per unit cell, while red dots form sublattice L_B with $N_B = 1$ site per unit cell. Nearest-neighbor hoppings are shown with the corresponding strength with the non-reciprocal inter-sublattice hopping, $\delta t = t_{AB} - t_{BA} \neq 0$.

identically. For instance,

$$\begin{aligned} (\Psi_{n,\mathbf{k},L}^{\pm})^{\dagger} \partial_{\mu} \Psi_{n,\mathbf{k},R}^{\pm} &= \\ \frac{1}{2\sqrt{1-\alpha^2}} \left(\frac{\pm\sqrt{1-\alpha}\phi_{n,\mathbf{k}}}{\sqrt{1+\alpha}\psi_{n,\mathbf{k}}} \right)^{\dagger} \left(\frac{\pm\sqrt{1+\alpha}\partial_{\mu}\phi_{n,\mathbf{k}}}{\sqrt{1-\alpha}\partial_{\mu}\psi_{n,\mathbf{k}}} \right) &= \\ \frac{\sqrt{1-\alpha^2}}{2\sqrt{1-\alpha^2}} (\phi_{n,\mathbf{k}}^{\dagger} \partial_{\mu} \phi_{n,\mathbf{k}} + \psi_{n,\mathbf{k}}^{\dagger} \partial_{\mu} \psi_{n,\mathbf{k}}) &= \\ \frac{(\phi_{n,\mathbf{k}}^{\dagger} \partial_{\mu} \phi_{n,\mathbf{k}} + \psi_{n,\mathbf{k}}^{\dagger} \partial_{\mu} \psi_{n,\mathbf{k}})}{2}, \end{aligned}$$

which is exactly the same result obtained in the purely Hermitian case. The same argument applies in this case for the flat-band states, since they have the same form as in the Hermitian case. As such, the chiral NH bipartite system inherits the trivial topology from its original parent model [102], when $\alpha \neq \pm 1$, which can be also directly verified by the fact that the NH QGT is fully symmetric, independently of the explicit form of $\phi_{n,\mathbf{k}}$ and $\psi_{n,\mathbf{k}}$.

Introducing sublattice-dependent chemical potentials does not change the structure of the flat-band eigenstates; they remain topologically trivial. In the dispersive sector, the QGT is still symmetric (hence zero Berry curvature), but the eigenstates acquire a non-separable α -dependence that leaves a clear imprint in the quantum metric, providing a sensitive diagnostic of spectral degeneracies (exceptional points) in the NH regime. Because closed-form expressions are cumbersome in general, we present explicit QGT results for the Lieb lattice, Fig. 2 in the main text.

S3. Non-Hermitian Lieb Lattice

The minimal number of fermionic degrees of freedom for the construction of a BCL such that $N_A - N_B > 0$ and $N_A, N_B > 0$ is *three*, with $N_A = 2$ and $N_B = 1$. In two dimensions, a natural realization is the Lieb lattice: a square lattice with three sites per unit cell and two interpenetrating sublattices: corner sites and edge-center sites (see Fig. 6). Introducing a hopping imbalance, the real-space Hamiltonian takes the form

$$H = \mu_A \sum_{\mathbf{r}} \sum_{i=1}^2 \hat{a}_{\mathbf{r},i}^\dagger \hat{a}_{\mathbf{r},i} + \mu_B \sum_{\mathbf{r}} \hat{b}_{\mathbf{r}}^\dagger \hat{b}_{\mathbf{r}} - \sum_{\mathbf{r}} \sum_{i=1}^2 \left(t_{AB} \hat{b}_{\mathbf{r}}^\dagger \hat{a}_{\mathbf{r}+\boldsymbol{\delta}_i,i} + t_{BA} \hat{a}_{\mathbf{r}+\boldsymbol{\delta}_i,i}^\dagger \hat{b}_{\mathbf{r}} \right),$$

where the operator $\hat{b}_{\mathbf{r}}^\dagger$ creates a fermion on the site \mathbf{r} in the sublattice L_B , while the operator $\hat{a}_{\mathbf{r},i}^\dagger$ creates a fermion on the two inequivalent sites $i = 1, 2$ that form the sublattice L_A . The vectors $\boldsymbol{\delta}_i = \pm(a/2) \mathbf{e}_{x,y}$ connect the nearest neighbor sites, with a as the distance between the nearest-neighbor sites on the sublattice L_B (red sites in Fig. 6). The hopping parameters $t_{AB} \neq t_{BA}$ are real, \mathbf{e}_x (\mathbf{e}_y) is the unit vector in the principal x (y) direction of the lattice.

This tight-binding model can be written in the Bloch form in terms of the operator $\Psi_{\mathbf{k}}^\dagger = (\hat{a}_{1,\mathbf{k}} \ \hat{a}_{2,\mathbf{k}} \ \hat{b}_{\mathbf{k}})$ as $H = \sum_{\mathbf{k}} \Psi_{\mathbf{k}}^\dagger h_{\mathbf{k}} \Psi_{\mathbf{k}}$, with

$$h_{\mathbf{k}} = \begin{pmatrix} \mu_A \mathbf{1}_2 & (1 + \alpha) S_{\mathbf{k}} \\ (1 - \alpha) S_{\mathbf{k}}^\dagger & \mu_B \end{pmatrix}, \quad (15)$$

where $S_{\mathbf{k}}^\dagger = -2\bar{t}(\cos(k_x a/2) \ \cos(k_y a/2))$, $\bar{t} = (t_{AB} + t_{BA})/2$ is the mean-value of the hopping amplitudes and $\alpha = \delta t / \bar{t} = (t_{AB} - t_{BA}) / (t_{AB} + t_{BA})$ is the dimensionless parameter tuning the NH effects induced by the non-reciprocal hoppings. Evidently, it shares the same generic structure of the main text, and therefore we can write explicitly its eigenstates and spectrum in terms of the non-zero singular eigenstates of $S_{\mathbf{k}}$,

$$\phi_{\mathbf{k}} = \frac{1}{\sqrt{\cos^2(k_x a/2) + \cos^2(k_y a/2)}} \begin{pmatrix} \cos(k_x a/2) \\ \cos(k_y a/2) \end{pmatrix},$$

$$\psi_{\mathbf{k}} = 1,$$

with eigenvalue $\epsilon_{\mathbf{k}} = -2\bar{t}\sqrt{\cos^2(k_x a/2) + \cos^2(k_y a/2)}$, following the notation of Sec. (S1). Additionally, there is also a zero-mode that spans the kernel of $S_{\mathbf{k}}^\dagger$, given by

$$\phi_{0,\mathbf{k}} = \frac{1}{\sqrt{\cos^2(k_x a/2) + \cos^2(k_y a/2)}} \begin{pmatrix} -\cos(k_y a/2) \\ \cos(k_x a/2) \end{pmatrix}.$$

With this, we are able now to write down the explicit form of the right and left eigenstates of the NH Bloch

Hamiltonian in Eq. (15) following the general procedure of Sec. S1.

An explicit calculation then shows that indeed the Berry curvature is zero for this system, just as was expected, and that there is a critical value for α for which the second flat band pinned at $\bar{\mu}$ starts to emerge, given in this case by

$$|\alpha| \geq \alpha_c = \sqrt{1 + \frac{\delta\mu^2}{8\bar{t}^2}}. \quad (16)$$

For $|\alpha| < \alpha_c$, $\Delta_{\mathbf{k}}$ is necessarily real-valued at every point of the BZ, provided by the fact that $\epsilon_{\mathbf{k}}^2 \leq 8\bar{t}^2$, with the equality holding at the Γ -point. As such, the spectrum for this system is purely real within the range of values $\alpha \in (-\alpha_c, \alpha_c)$, resembling the band structure of the Hermitian model, whilst beyond this regime the dispersive states start to collapse onto the exceptional flat band, although acquiring a finite lifetime proportional to $\Delta_{\mathbf{k}}^{-1}$.

* Corresponding author:vladimir.juricic@usm.cl

- [1] E. J. Bergholtz and Z. Liu, Topological flat band models and fractional chern insulators, *International Journal of Modern Physics B* **27**, 1330017 (2013).
- [2] S. A. Parameswaran, R. Roy, and S. L. Sondhi, Fractional quantum hall physics in topological flat bands, *Comptes Rendus Physique* **14**, 816 (2013), topological insulators / Isolants topologiques.
- [3] T. T. Heikkilä and G. E. Volovik, Flat bands as a route to high-temperature superconductivity in graphite, in *Basic Physics of Functionalized Graphite* (Springer, 2016) pp. 123–143.
- [4] G. E. Volovik, Graphite, graphene, and the flat band superconductivity, *JETP Letters* **107**, 516 (2018).
- [5] B. Roy and V. Jurić, Unconventional superconductivity in nearly flat bands in twisted bilayer graphene, *Phys. Rev. B* **99**, 121407 (2019).
- [6] Y. Cao, V. Fatemi, A. Demir, S. Fang, S. L. Tomarken, J. Y. Luo, J. D. Sanchez-Yamagishi, K. Watanabe, T. Taniguchi, E. Kaxiras, *et al.*, Correlated insulator behaviour at half-filling in magic-angle graphene superlattices, *Nature* **556**, 80 (2018).
- [7] Y. Cao, V. Fatemi, S. Fang, K. Watanabe, T. Taniguchi, E. Kaxiras, and P. Jarillo-Herrero, Unconventional superconductivity in magic-angle graphene superlattices, *Nature* **556**, 43 (2018).
- [8] Y. Cao, D. Rodan-Legrain, J. M. Park, N. F. Q. Yuan, K. Watanabe, T. Taniguchi, R. M. Fernandes, L. Fu, and P. Jarillo-Herrero, Nematicity and competing orders in superconducting magic-angle graphene, *Science* **372**, 264 (2021).
- [9] Y. Xie, A. T. Pierce, J. M. Park, D. E. Parker, E. Khalaf, P. Ledwith, Y. Cao, S. H. Lee, S. Chen, P. R. Forrester, *et al.*, Fractional chern insulators in magic-angle twisted bilayer graphene, *Nature* **600**, 439 (2021).
- [10] J. M. Park, Y. Cao, K. Watanabe, T. Taniguchi, and P. Jarillo-Herrero, Flavour hund's coupling, chern gaps and charge diffusivity in moiré graphene, *Nature* **592**, 43 (2021).

- [11] I. Das, X. Lu, J. Herzog-Arbeitman, Z.-D. Song, K. Watanabe, T. Taniguchi, B. A. Bernevig, and D. K. Efetov, Symmetry-broken chern insulators and rashba-like landau-level crossings in magic-angle bilayer graphene, *Nature Physics* **17**, 710 (2021).
- [12] Y. Choi, H. Kim, Y. Peng, A. Thomson, C. Lewandowski, R. Polski, Y. Zhang, H. S. Arora, K. Watanabe, T. Taniguchi, *et al.*, Correlation-driven topological phases in magic-angle twisted bilayer graphene, *Nature* **589**, 536 (2021).
- [13] M. Sánchez Sánchez, I. Díaz, J. González, and T. Stauber, Nematic versus kekulé phases in twisted bilayer graphene under hydrostatic pressure, *Phys. Rev. Lett.* **133**, 266603 (2024).
- [14] E. Suárez Morell, J. D. Correa, P. Vargas, M. Pacheco, and Z. Barticevic, Flat bands in slightly twisted bilayer graphene: Tight-binding calculations, *Phys. Rev. B* **82**, 121407 (2010).
- [15] R. Bistritzer and A. H. MacDonald, Moiré bands in twisted double-layer graphene, *Proceedings of the National Academy of Sciences* **108**, 12233 (2011).
- [16] J. M. B. Lopes dos Santos, N. M. R. Peres, and A. H. Castro Neto, Graphene bilayer with a twist: Electronic structure, *Phys. Rev. Lett.* **99**, 256802 (2007).
- [17] J. Kang and O. Vafek, Symmetry, maximally localized wannier states, and a low-energy model for twisted bilayer graphene narrow bands, *Phys. Rev. X* **8**, 031088 (2018).
- [18] H. C. Po, L. Zou, T. Senthil, and A. Vishwanath, Faithful tight-binding models and fragile topology of magic-angle bilayer graphene, *Phys. Rev. B* **99**, 195455 (2019).
- [19] M. P. Shores, E. A. Nytko, B. M. Bartlett, and D. G. Nocera, A structurally perfect $s = 1/2$ kagomé antiferromagnet, *Journal of the american chemical society* **127**, 13462 (2005).
- [20] P. Mendels and F. Bert, Quantum kagome antiferromagnet $\text{ZnCu}_3(\text{OH})_6\text{Cl}_2$, *Journal of the Physical Society of Japan* **79**, 011001 (2010).
- [21] T.-H. Han, J. S. Helton, S. Chu, D. G. Nocera, J. A. Rodriguez-Rivera, C. Broholm, and Y. S. Lee, Fractionalized excitations in the spin-liquid state of a kagome-lattice antiferromagnet, *Nature* **492**, 406 (2012).
- [22] I. Mazin, H. O. Jeschke, F. Lechermann, H. Lee, M. Fink, R. Thomale, and R. Valentí, Theoretical prediction of a strongly correlated dirac metal, *Nature communications* **5**, 4261 (2014).
- [23] S. Lisi, X. Lu, T. Benschop, T. A. de Jong, P. Stepanov, J. R. Duran, F. Margot, I. Cucchi, E. Cappelli, A. Hunter, *et al.*, Observation of flat bands in twisted bilayer graphene, *Nature Physics* **17**, 189 (2021).
- [24] I. Hase, Y. Higashi, H. Eisaki, and K. Kawashima, New three-dimensional flat band candidate materials $\text{Pb}_2\text{As}_2\text{O}_7$ and $\text{Pb}_2\text{Sn}_2\text{O}_7$, *Scientific Reports* **14**, 26532 (2024).
- [25] Y. Nakata, T. Okada, T. Nakanishi, and M. Kitano, Observation of flat band for terahertz spoof plasmons in a metallic kagomé lattice, *Phys. Rev. B* **85**, 205128 (2012).
- [26] S. Kajiwar, Y. Urade, Y. Nakata, T. Nakanishi, and M. Kitano, Observation of a nonradiative flat band for spoof surface plasmons in a metallic lieb lattice, *Phys. Rev. B* **93**, 075126 (2016).
- [27] H. Wang, B. Yang, W. Xu, Y. Fan, Q. Guo, Z. Zhu, and C. T. Chan, Highly degenerate photonic flat bands arising from complete graph configurations, *Phys. Rev. A* **100**, 043841 (2019).
- [28] H. Takeda, T. Takashima, and K. Yoshino, Flat photonic bands in two-dimensional photonic crystals with kagome lattices, *Journal of Physics: Condensed Matter* **16**, 6317 (2004).
- [29] R. A. Vicencio, C. Cantillano, L. Morales-Inostroza, B. Real, C. Mejía-Cortés, S. Weimann, A. Szameit, and M. I. Molina, Observation of localized states in lieb photonic lattices, *Phys. Rev. Lett.* **114**, 245503 (2015).
- [30] F. Baboux, L. Ge, T. Jacqmin, M. Biondi, E. Galopin, A. Lemaître, L. Le Gratiet, I. Sagnes, S. Schmidt, H. E. Türeci, A. Amo, and J. Bloch, Bosonic condensation and disorder-induced localization in a flat band, *Phys. Rev. Lett.* **116**, 066402 (2016).
- [31] S. Mukherjee, A. Spracklen, D. Choudhury, N. Goldman, P. Öhberg, E. Andersson, and R. R. Thomson, Observation of a localized flat-band state in a photonic lieb lattice, *Phys. Rev. Lett.* **114**, 245504 (2015).
- [32] Y.-C. He, F. Grusdt, A. Kaufman, M. Greiner, and A. Vishwanath, Realizing and adiabatically preparing bosonic integer and fractional quantum hall states in optical lattices, *Phys. Rev. B* **96**, 201103 (2017).
- [33] N. R. Cooper, J. Dalibard, and I. B. Spielman, Topological bands for ultracold atoms, *Rev. Mod. Phys.* **91**, 015005 (2019).
- [34] C. Zeng, Y.-R. Shi, Y.-Y. Mao, F.-F. Wu, Y.-J. Xie, T. Yuan, H.-N. Dai, and Y.-A. Chen, Observation of flat-band localized state in a one-dimensional diamond momentum lattice of ultracold atoms, *Chinese Physics B* **33**, 010303 (2023).
- [35] W. Sui, W. Han, Z. V. Han, Z. Meng, and J. Zhang, Topologically nontrivial and trivial flat bands via weak and strong interlayer coupling in twisted bilayer honeycomb optical lattices for ultracold atoms, *Phys. Rev. A* **111**, 063306 (2025).
- [36] D.-S. Ma, Y. Xu, C. S. Chiu, N. Regnault, A. A. Houck, Z. Song, and B. A. Bernevig, Spin-orbit-induced topological flat bands in line and split graphs of bipartite lattices, *Phys. Rev. Lett.* **125**, 266403 (2020).
- [37] D. Călugăru, A. Chew, L. Elcoro, Y. Xu, N. Regnault, Z.-D. Song, and B. A. Bernevig, General construction and topological classification of crystalline flat bands, *Nature Physics* **18**, 185 (2022).
- [38] Y. Hwang, J.-W. Rhim, and B.-J. Yang, General construction of flat bands with and without band crossings based on wave function singularity, *Phys. Rev. B* **104**, 085144 (2021).
- [39] H. Kim, C.-g. Oh, and J.-W. Rhim, General construction scheme for geometrically nontrivial flat band models, *Communications Physics* **6**, 305 (2023).
- [40] D. Leykam, S. Flach, and Y. D. Chong, Flat bands in lattices with non-hermitian coupling, *Phys. Rev. B* **96**, 064305 (2017).
- [41] H. Ramezani, Non-hermiticity-induced flat band, *Phys. Rev. A* **96**, 011802 (2017).
- [42] A. Y. Zyuzin and A. Y. Zyuzin, Flat band in disorder-driven non-hermitian weyl semimetals, *Phys. Rev. B* **97**, 041203 (2018).
- [43] S. M. Zhang and L. Jin, Flat band in two-dimensional non-hermitian optical lattices, *Phys. Rev. A* **100**, 043808 (2019).
- [44] L. Jin, Flat band induced by the interplay of synthetic magnetic flux and non-hermiticity, *Phys. Rev. A* **99**,

- 033810 (2019).
- [45] W. Maimaiti and A. Andreanov, Non-hermitian flat-band generator in one dimension, *Phys. Rev. B* **104**, 035115 (2021).
 - [46] L. Ding, Z. Lin, S. Ke, B. Wang, and P. Lu, Non-hermitian flat bands in rhombic microring resonator arrays, *Opt. Express* **29**, 24373 (2021).
 - [47] S. Talkington and M. Claassen, Dissipation-induced flat bands, *Phys. Rev. B* **106**, L161109 (2022).
 - [48] X.-P. Jiang, W. Zeng, Y. Hu, and P. Liu, Exact non-hermitian mobility edges and robust flat bands in two-dimensional lieb lattices with imaginary quasiperiodic potentials, *New Journal of Physics* **26**, 083020 (2024).
 - [49] I. Amelio and N. Goldman, Lasing in non-hermitian flat bands: Quantum geometry, coherence, and the fate of kardar-parisi-zhang physics, *Phys. Rev. Lett.* **132**, 186902 (2024).
 - [50] A. Banerjee, A. Bandyopadhyay, R. Sarkar, and A. Narayan, Non-hermitian topology and flat bands via an exact real-space decimation scheme, *Phys. Rev. B* **110**, 085431 (2024).
 - [51] C. A. Leong and B. Roy, Non-hermitian catalysis of density-wave orders on euclidean and hyperbolic lattices (2025), [arXiv:2501.18591 \[cond-mat.str-el\]](https://arxiv.org/abs/2501.18591).
 - [52] Z. Gong, Y. Ashida, K. Kawabata, K. Takasan, S. Higashikawa, and M. Ueda, Topological Phases of Non-Hermitian Systems, *Phys. Rev. X* **8**, 031079 (2018).
 - [53] L. E. F. Foa Torres, Perspective on topological states of non-hermitian lattices, *Journal of Physics: Materials* **3**, 014002 (2019).
 - [54] E. J. Bergholtz, J. C. Budich, and F. K. Kunst, Exceptional topology of non-hermitian systems, *Rev. Mod. Phys.* **93**, 015005 (2021).
 - [55] W. D. Heiss, The physics of exceptional points, *Journal of Physics A: Mathematical and Theoretical* **45**, 444016 (2012).
 - [56] W. Hu, H. Wang, P. P. Shum, and Y. D. Chong, Exceptional points in a non-hermitian topological pump, *Phys. Rev. B* **95**, 184306 (2017).
 - [57] V. M. Martinez Alvarez, J. E. Barrios Vargas, and L. E. F. Foa Torres, Non-hermitian robust edge states in one dimension: Anomalous localization and eigenspace condensation at exceptional points, *Phys. Rev. B* **97**, 121401 (2018).
 - [58] K. Kawabata, T. Bessho, and M. Sato, Classification of exceptional points and non-hermitian topological semimetals, *Phys. Rev. Lett.* **123**, 066405 (2019).
 - [59] V. Kozii and L. Fu, Non-Hermitian topological theory of finite-lifetime quasiparticles: Prediction of bulk Fermi arc due to exceptional point, *Phys. Rev. B* **109**, 235139 (2024).
 - [60] V. Jurić and B. Roy, Yukawa-Lorentz symmetry in non-Hermitian Dirac materials, *Communications Physics* **7**, 169 (2024).
 - [61] X.-J. Yu, Z. Pan, L. Xu, and Z.-X. Li, Non-hermitian strongly interacting dirac fermions, *Phys. Rev. Lett.* **132**, 116503 (2024).
 - [62] S. A. Murshed and B. Roy, Quantum electrodynamics of non-Hermitian Dirac fermions, *Journal of High Energy Physics* **2024**, 1 (2024).
 - [63] S. A. Murshed and B. Roy, Yukawa-Lorentz symmetry of interacting non-Hermitian birefringent Dirac fermions, *SciPost Phys.* **18**, 073 (2025).
 - [64] S. Pino-Alarcón and V. Jurić, Yukawa-lorentz symmetry of tilted non-hermitian dirac semimetals at quantum criticality, *Phys. Rev. B* **111**, 195126 (2025).
 - [65] J. P. Esparza and V. Jurić, Exceptional magic angles in non-hermitian twisted bilayer graphene, *Phys. Rev. Lett.* **134**, 226602 (2025).
 - [66] Y. Huang, Exceptional topology in non-hermitian twisted bilayer graphene, *Phys. Rev. B* **111**, 085120 (2025).
 - [67] L. Jin, Topological phases and edge states in a non-hermitian trimerized optical lattice, *Phys. Rev. A* **96**, 032103 (2017).
 - [68] X. Zhou, S. K. Gupta, Z. Huang, Z. Yan, P. Zhan, Z. Chen, M. Lu, and Z. Wang, Optical lattices with higher-order exceptional points by non-hermitian coupling, *Applied Physics Letters* **113**, <https://doi.org/10.1063/1.5043279> (2018).
 - [69] M. Pan, H. Zhao, P. Miao, S. Longhi, and L. Feng, Photonic zero mode in a non-hermitian photonic lattice, *Nature communications* **9**, 1308 (2018).
 - [70] W. Song, W. Sun, C. Chen, Q. Song, S. Xiao, S. Zhu, and T. Li, Breakup and recovery of topological zero modes in finite non-hermitian optical lattices, *Phys. Rev. Lett.* **123**, 165701 (2019).
 - [71] Y. Zhang, X. Dai, and Y. Xiang, Topological hierarchy in non-hermitian three-dimensional photonic crystals, *Phys. Rev. B* **110**, 104103 (2024).
 - [72] L. Li, C. H. Lee, and J. Gong, Topological switch for non-hermitian skin effect in cold-atom systems with loss, *Phys. Rev. Lett.* **124**, 250402 (2020).
 - [73] L. Zhou, H. Li, W. Yi, and X. Cui, Engineering non-hermitian skin effect with band topology in ultracold gases, *Communications Physics* **5**, 252 (2022).
 - [74] Q. Liang, D. Xie, Z. Dong, H. Li, H. Li, B. Gadway, W. Yi, and B. Yan, Dynamic signatures of non-hermitian skin effect and topology in ultracold atoms, *Phys. Rev. Lett.* **129**, 070401 (2022).
 - [75] Z.-F. Cai, T. Liu, and Z. Yang, Non-hermitian skin effect in periodically driven dissipative ultracold atoms, *Phys. Rev. A* **109**, 063329 (2024).
 - [76] E. Zhao, Z. Wang, C. He, T. F. J. Poon, K. K. Pak, Y.-J. Liu, P. Ren, X.-J. Liu, and G.-B. Jo, Two-dimensional non-hermitian skin effect in an ultracold fermi gas, *Nature* **637**, 565 (2025).
 - [77] S. M. Rafi-Ul-Islam, H. Sahin, Z. B. Siu, and M. B. A. Jalil, Interfacial skin modes at a non-hermitian heterojunction, *Phys. Rev. Res.* **4**, 043021 (2022).
 - [78] J. Wu, X. Huang, Y. Yang, W. Deng, J. Lu, W. Deng, and Z. Liu, Non-hermitian second-order topology induced by resistances in electric circuits, *Phys. Rev. B* **105**, 195127 (2022).
 - [79] B. Liu, Y. Li, B. Yang, X. Shen, Y. Yang, Z. H. Hang, and M. Ezawa, Experimental observation of non-hermitian higher-order skin interface states in topological electric circuits, *Phys. Rev. Res.* **5**, 043034 (2023).
 - [80] K. Ochkan, R. Chaturvedi, V. Könye, L. Veyrat, R. Giraud, D. Mailly, A. Cavanna, U. Gennser, E. M. Hankiewicz, B. Büchner, *et al.*, Non-hermitian topology in a multi-terminal quantum hall device, *Nature Physics* **20**, 395 (2024).
 - [81] W. Zhang, F. Di, and X. Zhang, Non-hermitian global synchronization, *Advanced Science* **12**, 2408460 (2025).
 - [82] S. Jana and L. Sirota, Invisible tunneling through non-hermitian barriers in nonreciprocal lattices, *Phys. Rev. B* **111**, L100301 (2025).

- [83] H. Sahin, M. B. A. Jalil, and C. H. Lee, Topoelectrical circuits—recent experimental advances and developments, *APL Electronic Devices* **1**, 021503 (2025).
- [84] T. Yoshida, K. Kudo, and Y. Hatsugai, Non-hermitian fractional quantum hall states, *Scientific reports* **9**, 16895 (2019).
- [85] K. Yamamoto, M. Nakagawa, K. Adachi, K. Takasan, M. Ueda, and N. Kawakami, Theory of non-hermitian fermionic superfluidity with a complex-valued interaction, *Phys. Rev. Lett.* **123**, 123601 (2019).
- [86] D.-W. Zhang, Y.-L. Chen, G.-Q. Zhang, L.-J. Lang, Z. Li, and S.-L. Zhu, Skin superfluid, topological mott insulators, and asymmetric dynamics in an interacting non-hermitian aubry-andré-harper model, *Phys. Rev. B* **101**, 235150 (2020).
- [87] T. Liu, J. J. He, T. Yoshida, Z.-L. Xiang, and F. Nori, Non-Hermitian topological Mott insulators in one-dimensional fermionic superlattices, *Phys. Rev. B* **102**, 235151 (2020).
- [88] K. Kawabata, S. Higashikawa, Z. Gong, Y. Ashida, and M. Ueda, Topological unification of time-reversal and particle-hole symmetries in non-Hermitian physics, *Nature communications* **10**, 297 (2019).
- [89] J. Cayao and A. M. Black-Schaffer, Exceptional odd-frequency pairing in non-hermitian superconducting systems, *Phys. Rev. B* **105**, 094502 (2022).
- [90] A. K. Ghosh and T. Nag, Non-hermitian higher-order topological superconductors in two dimensions: Statics and dynamics, *Phys. Rev. B* **106**, L140303 (2022).
- [91] Z. Wang, L.-J. Lang, and L. He, Emergent mott insulators and non-hermitian conservation laws in an interacting bosonic chain with noninteger filling and nonreciprocal hopping, *Phys. Rev. B* **105**, 054315 (2022).
- [92] C. Li, Y. Wu, and W.-M. Liu, Non-hermitian superfluid–mott-insulator transition in the one-dimensional zigzag bosonic chains, *Phys. Rev. B* **109**, 214306 (2024).
- [93] T. Yoshida, S.-B. Zhang, T. Neupert, and N. Kawakami, Non-hermitian mott skin effect, *Phys. Rev. Lett.* **133**, 076502 (2024).
- [94] X. Ji, W. Ding, Y. Chen, and X. Yang, Non-hermitian second-order topological superconductors, *Phys. Rev. B* **109**, 125420 (2024).
- [95] T. Shi, S. Wang, Z. Zheng, and W. Zhang, Two-dimensional non-hermitian fermionic superfluidity with spin imbalance, *Phys. Rev. A* **109**, 063306 (2024).
- [96] S. Takemori, K. Yamamoto, and A. Koga, Theory of non-hermitian fermionic superfluidity on a honeycomb lattice: Interplay between exceptional manifolds and van hove singularity, *Phys. Rev. B* **109**, L060501 (2024).
- [97] E. H. Lieb, Two theorems on the hubbard model, *Phys. Rev. Lett.* **62**, 1201 (1989).
- [98] See Supplementary Materials including Sec. S1: Explicit form of the eigenstates for the non-Hermitian bipartite lattice both in the chiral case and with chemical potential offset at each sublattice; Sec. S2: Details on the analysis of the quantum geometric tensor; Sec. S3: An explicit example of our method in terms of the two-dimensional Lieb lattice with non-reciprocal hoppings., .
- [99] H. Shen, B. Zhen, and L. Fu, Topological band theory for non-hermitian hamiltonians, *Phys. Rev. Lett.* **120**, 146402 (2018).
- [100] Y.-Q. Zhu, W. Zheng, S.-L. Zhu, and G. Palumbo, Band topology of pseudo-hermitian phases through tensor berry connections and quantum metric, *Phys. Rev. B* **104**, 205103 (2021).
- [101] Y.-M. R. Hu, E. A. Ostrovskaya, and E. Estrecho, Generalized quantum geometric tensor in a non-hermitian exciton-polariton system, *Opt. Mater. Express* **14**, 664 (2024).
- [102] A. Kruchkov, Quantum geometry, flat Chern bands, and Wannier orbital quantization, *Phys. Rev. B* **105**, L241102 (2022).